HTML ABSTRACT + LINKS

Imaging and quantifying mixing in a model droplet micromixer

Z. B. Stone and H. A. Stone[a)]
Division of Engineering and Applied Sciences, Harvard University, Cambridge, Massachusetts 02138

(Received 11 November 2004; accepted 19 April 2005; published online 3 June 2005)

Rapid mixing is essential in a variety of microfluidic applications but is often difficult to achieve at low Reynolds numbers. Inspired by a recently developed microdevice that mixes reagents in droplets, which simply flow along a periodic serpentine channel [H. Song, J. D. Tice, and R. F. Ismagilov, "A microfluidic system for controlling reaction networks in time," Angew. Chem. Int. Ed. **42**, 767 (2003)], we investigate a model "droplet mixer." The model consists of a spherical droplet immersed in a periodic sequence of distinct external flows, which are superpositions of uniform and shear flows. We label the fluid inside the droplet with two colors and visualize mixing with a method we call "backtrace imaging," which allows us to render cross sections of the droplet at arbitrary times during the mixing cycle. To analyze our results, we present a novel scalar measure of mixing that permits us to locate sets of parameters that optimize mixing over a small number of flow cycles. © *2005 American Institute of Physics*. [DOI: 10.1063/1.1929547]

I. INTRODUCTION

Mixing of fluids underlies such diverse applications as stirring cream into a cup of coffee, tracking pollutants in large-scale river or atmospheric flows, and combining molten polymers to form industrially useful compounds. Mixing has also proven to be a rich subject for theoretical research, and connections have been forged with nonlinear and chaotic dynamical systems theory.[1–3] Rapid fluid mixing is an especially important challenge in modern microfluidic applications.[4] In particular, one approach to small-scale chemistry employs aqueous droplets immersed in an immiscible liquid both as reagent transport systems and as isolated chemical reactors.[5] The droplet fluid must mix thoroughly for chemical reactions to proceed efficiently, or to determine chemical kinetic rate constants accurately, but diffusion alone would mix fluids in a stationary droplet very slowly.[6] The serpentine channel illustrated in Fig. 1, in which aqueous solutions are injected as droplets into a pressure-driven flow of immiscible oil, offers one route to accelerate mixing in droplets by convection.[5,7] The varying geometry of the channel induces a series of distinct internal flows inside each droplet that stir its contents. Here we investigate a low-Reynolds-number model droplet stirrer or mixer inspired by this serpentine microfluidic device. We also discuss a novel technique of imaging three-dimensional stirring flows and provide a new idea for quantifying via a single scalar measure the degree of mixing as a function of time in purely kinematic simulations.

The subject of low-Reynolds-number stirring internal to isolated liquid droplets was first investigated theoretically by Bajer and Moffatt,[8] who clearly identified the possibility of chaotic streamlines in a steady three-dimensional flow internal to a droplet. Stone *et al.*[9] and Kroujiline and Stone[10] extended this work to the case of realistic velocity distributions associated with steady uniform and linear flows outside an isolated droplet in an unbounded fluid domain. Bryden and Brenner[11] investigated mass transfer for droplet flows with chaotic streamlines, and Ward and Homsy[12] addressed mixing inside droplets due to electrically driven flows, including some aspects of the time evolution of the mixing. Our work extends these previous studies in that we investigate time-periodic flows inside a droplet, which mimic several of the basic features of the serpentine mixer in Fig. 1. The reader may wish to glance ahead to the figures in Sec. VI to see these techniques applied. The ideas for visualizing and quantifying mixing presented here could also be applied directly to other mixing flows.

We begin by introducing in Sec. II the model for the time-dependent flow inside a drop, inspired by the serpentine channel shown in Fig. 1. The detailed equations for the trajectories of fluid elements and the parameters of the model are given in Sec. III. In Sec. IV, we describe a procedure we call "backtrace imaging" for efficiently visualizing the time evolution of a mixing flow. In order to quantify the degree of mixing, we introduce a scalar measure, or mixing number, in Sec. V. Finally, in Sec. VI, we use the method of backtrace imaging and the mixing number to study mixing visually and quantitatively in our model system.

II. QUALITATIVE DESCRIPTION OF MODEL FLOW

The actual flow field inside a droplet carried by a second immiscible liquid down a serpentine channel with a rectangular cross section is very complicated, especially when the diameter of the undeformed droplet is comparable to or larger than the channel width. To construct a simple model of the flow internal to the droplet, we choose to focus on the most basic features of the serpentine channel mixer: curves and straight segments of varying lengths; note that it has been observed in experiments that the mixing characteristics are not significantly affected, for example, by whether a turn is sharp or smooth.[7] Furthermore, we assume that the flow is

[a)]Author to whom correspondence should be addressed. Electronic mail: has@deas.harvard.edu

 © 2005 American Institute of Physics

Downloaded 22 Jul 2005 to 128.103.60.225. Redistribution subject to AIP license or copyright, see http://pof.aip.org/pof/copyright.jsp

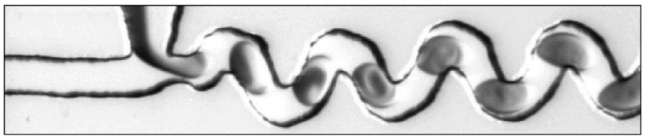

FIG. 1. A rapid microfluidic mixing system developed by Song, Tice, and Ismagilov (Ref. 5). Two aqueous solutions are injected into a stream of immiscible oil (viscosity = 5.10 mPa s) and pinch off into droplets that flow to the right down a serpentine channel, which is 28 μm wide and 45 μm deep. Figure reproduced from Ref. 5.

at low Reynolds number, which is a good approximation for the recent experiments.[5] Because each droplet in the serpentine channel device in Fig. 1 is created with fluid of one color filling roughly half of the droplet and the same fluid of another color filling the remaining half, we use that initial condition in our simulation.

The idealized mixer consists of a periodic sequence of four channel segments connected in the following order: a curve, a straight segment, a reverse curve, and another straight segment. Neglecting transitional flows as the droplet moves from one segment to another, each segment corresponds to a particular steady flow pattern inside the droplet. We map each channel segment to an unbounded external flow that can be applied analytically to a spherical droplet, thus capturing elements of the actual droplet flow. In this approximate correspondence between the model and the actual serpentine droplet mixer, the durations of the external flows in the model represent the lengths of the channel segments in the serpentine device. We choose a uniform external flow to represent the straight channel segments, since the streamlines induced in a droplet by such a flow are qualitatively similar to numerically calculated streamlines inside a droplet moving down a straight circular pipe.[13] For the curved channel segments, our main concern was to capture some change in velocity across the droplet due to the curve, and we accomplish this with an external shear flow superimposed on an external uniform flow. The sign of the shear alternates from one shear flow segment to the next shear segment to imitate the sequence of curves and reverse curves in the serpentine channel.

Combining all of these elements, our model mixer consists of a periodic sequence of four unbounded external flows applied to a spherical droplet at low Reynolds number: a superposition of uniform and shear flow, a uniform flow, a superposition of uniform and opposite-signed shear flow, and a uniform flow. Figure 2 compares the serpentine mixer with our model droplet mixer. As in the serpentine droplet mixer, these external flows in our model induce a sequence of steady flow patterns inside the droplet that mix its contents. As is standard in studies of chaotic advection, our model includes kinematics only; we do not account for molecular diffusion. Though it should be possible to simulate the serpentine channel mixer accurately with computationally intensive numerical methods, we choose to work with this simple model to explore stirring rapidly and interactively in a three-dimensional system. A two-dimensional numerical investigation of this system is reported by Muradoglu and Stone.[14]

III. EQUATIONS OF MOTION AND MODEL PARAMETERS

The equations of motion for fluid elements in a droplet immersed in an external uniform or shear flow are known analytically. In the limit of zero Reynolds number, these flows can be combined by superposition. Let $\lambda = \hat{\mu}/\mu$, where $\hat{\mu}$ is the viscosity of the fluid inside the drop and μ is the viscosity of the fluid outside, and let $r^2 = \mathbf{x}\cdot\mathbf{x}$, where $\mathbf{x}$ denotes the position vector relative to the center of the droplet. We nondimensionalize lengths by the drop radius a, velocities by the speed of the uniform flow U, and time by a/U; from now on, all variables are dimensionless. Also, we choose the z axis to be parallel with the direction of the uniform flow. In the case of uniform external flow (the Hadamard–Rybczynski problem), the trajectory $[x(t), y(t), z(t)]$ of a fluid particle inside the droplet is given by[10]

$$\dot{\mathbf{x}} = \mathbf{u}(\mathbf{x}) = \frac{\hat{\mathbf{U}}}{2(1+\lambda)} \cdot [(2r^2 - 1)\mathbf{I} - \mathbf{xx}], \tag{1a}$$

or

$$\dot{x} = \frac{zx}{2(1+\lambda)}, \tag{1b}$$

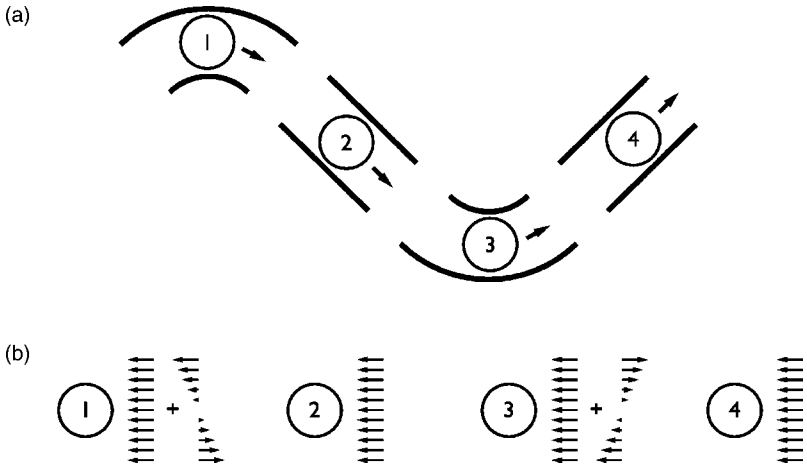

FIG. 2. A comparison of the serpentine channel mixer with our analytical model of a droplet mixer. Though the model does not represent the complex flow in the serpentine mixer, it mimics the mixer's four-step periodic flow pattern. (a) The serpentine channel mixer broken down into a periodic sequence of four segments: a curve, a straight segment, a reverse curve, and a second straight segment. (b) The sequence of four external flows applied to a spherical droplet in the model mixer, illustrated in the reference frame of the droplet: a superposition of uniform and shear flow, a uniform flow, a superposition of uniform and opposite-signed shear flow, and a uniform flow. For simplicity, we neglect transitional flows.

Downloaded 22 Jul 2005 to 128.103.60.225. Redistribution subject to AIP license or copyright, see http://pof.aip.org/pof/copyright.jsp

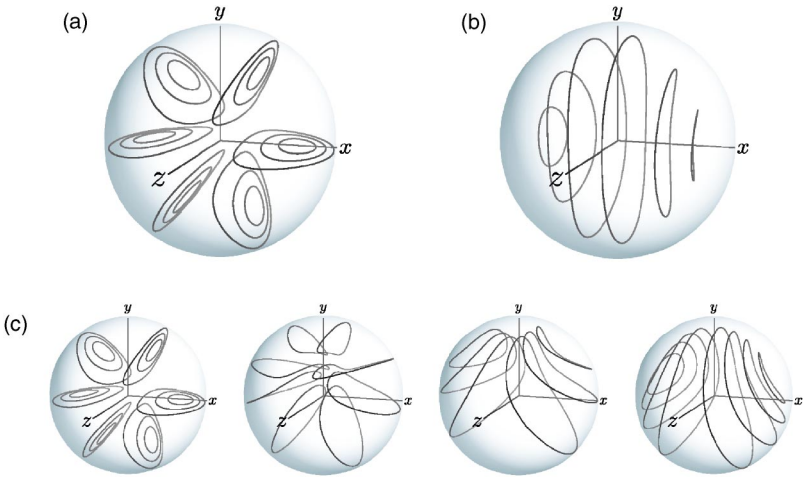

FIG. 3. Three-dimensional streamlines of the flow induced in a spherical droplet immersed in various external flows; the z axis is the primary flow direction. (a) Streamlines of Hadamard–Rybczynski flow induced in a droplet by a uniform external flow. (b) Streamlines inside a droplet induced by an external shear flow. (c) Streamlines inside a droplet induced by a superposition of external uniform and shear flows. The parameter λ is fixed at 1, and the dimensionless parameter β, which measures the relative strength of the shear and uniform flows, increases from 0 to 0.6 in increments of 0.2.

$$\dot{y} = \frac{zy}{2(1+\lambda)}, \tag{1c}$$

$$\dot{z} = \frac{1 - 2r^2 + z^2}{2(1+\lambda)}, \tag{1d}$$

where dots denote time derivatives and $\hat{\mathbf{U}} = -\mathbf{e}_z$.

Next, consider an external shear flow of the form $u_z = Gy$. We nondimensionalize lengths and velocities as above, and we define the nondimensional parameter $\beta = Ga/U$, which sets the strength of the shear flow in comparison with the uniform flow. The equations of motion for a fluid particle inside a droplet immersed in an external shear flow are[10]

$$\dot{\mathbf{x}} = \mathbf{u}(\mathbf{x}) = \frac{\beta(\mathbf{E}\cdot\mathbf{x})}{2(1+\lambda)}[(5r^2-3)\mathbf{I} - 2\mathbf{x}\mathbf{x}] + \frac{\beta}{2}\omega \wedge \mathbf{x}, \tag{2a}$$

or

$$\dot{x} = -\frac{\beta xyz}{(1+\lambda)}, \tag{2b}$$

$$\dot{y} = \frac{\beta}{2(1+\lambda)}\left[(5r^2-3)\frac{z}{2} - 2y^2 z\right] - \beta\frac{z}{2}, \tag{2c}$$

$$\dot{z} = \frac{\beta}{2(1+\lambda)}\left[(5r^2-3)\frac{y}{2} - 2z^2 y\right] + \beta\frac{y}{2}, \tag{2d}$$

where $\mathbf{E}$ and ω denote, respectively, the rate of strain tensor and vorticity vector of the shear flow. By superposition, we may add Eqs. (1) and (2) to produce an equation for the trajectory of a fluid particle inside a droplet immersed in combined uniform and shear external flows. All numerical integrations reported in this paper were performed with a fifth-order Runge–Kutta routine.[15] Streamlines of the flow induced inside a droplet by this combined external flow at various values of β are compared with streamlines of the flow induced by uniform and shear external flows in Fig. 3.

Several parameters control the model flow in addition to the viscosity ratio λ and the dimensionless shear rate β. Each of the individual segments in the cycle of flows in the model must be assigned a duration of dimensionless time. In the case of periodic cycles, each uniform flow segment is given a constant duration τ_t, and each uniform and shear segment is given a constant duration τ_s. The sign of β alternates from one shear segment to the next, imitating the alternating curves and reverse curves in the serpentine channel mixer. Our model can also accommodate nonperiodic sequences of segment durations.

Before providing detailed simulation results, in the next two sections we discuss the technique we use to image mixing in the droplet and a method for quantifying the degree of mixing via a scalar measure.

IV. IMAGING MIXING: THE BACKTRACE METHOD

Although it is common to report suitably chosen Poincaré sections to characterize the degree of mixing caused by a flow, such approaches give no indication of the time evolution of the actual mixing process.[16] Hence, we render cross sections of the droplet and three-dimensional grids of sample points throughout the mixing cycle. This kind of direct imaging is often performed in simulations by initializing large numbers of tracer particles in a flow, propagating them forwards in time, and plotting their evolving positions. However, direct imaging in this manner has certain drawbacks. First, a uniform grid of tracer particles is unlikely to stay even roughly uniform as time progresses, especially not in a chaotic mixing flow. In a three-dimensional flow this problem is especially acute, and it is computationally expensive to increase the density of tracer particles to compensate. Thus, we developed a backtrace imaging method to render uniformly sampled cross sections and three-dimensional grids at arbitrary times in the mixing process. We have since found similar ideas mentioned in a recent paper[17] and used by Gilbert in Ref. 18; see also Ref. 19 for a related mapping technique.

Using the equations of Sec. III, Fig. 4 compares an image produced by forward evolution of tracer particles to one generated by the backtrace imaging procedure. The two techniques required almost identical computational effort since approximately the same number of tracer particles were propagated for the same duration of dimensionless time to produce each image. Though both images clearly display the same qualitative features, the forward evolution method

Downloaded 22 Jul 2005 to 128.103.60.225. Redistribution subject to AIP license or copyright, see http://pof.aip.org/pof/copyright.jsp

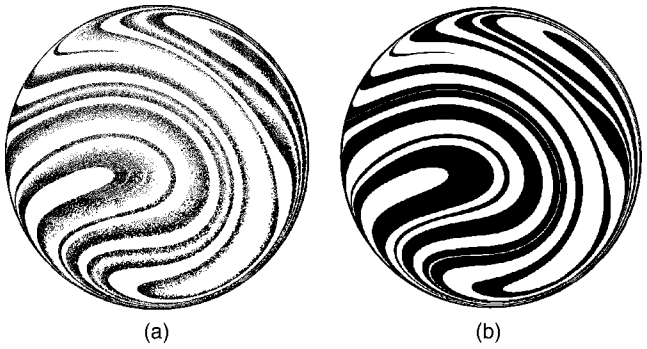

FIG. 4. A comparison of cross sections in the $x=0$ plane rendered (a) by forward evolution of tracer particles and (b) by backtrace imaging. The images were produced with nearly identical computational effort, since almost the same number of particles were propagated for the same length of time in each image. (The number of particles used to produce the forward evolution image was 283 032, and 281 760 particles were used to generate the backtrace image.) The cross sections were rendered at time $\tau=40$ in the mixing process, and the other parameters were $\tau_s=3$, $\tau_t=3$, $\beta=2/3$, and $\lambda=1$. Image (a) illustrates the nonuniformities that rapidly develop when a uniform grid of tracer particles is propagated forward in a mixing flow. The backtracing technique, by contrast, accurately colors every pixel in the droplet. This cross section in the $x=0$ plane was chosen for comparison because it lies along a plane of symmetry in the model, so fluid particles launched in the plane stay in the plane. A grid of particles in any other cross section would disperse nonuniformly in three dimensions when integrated forward in time, making backtrace imaging the only feasible way to image the cross section.

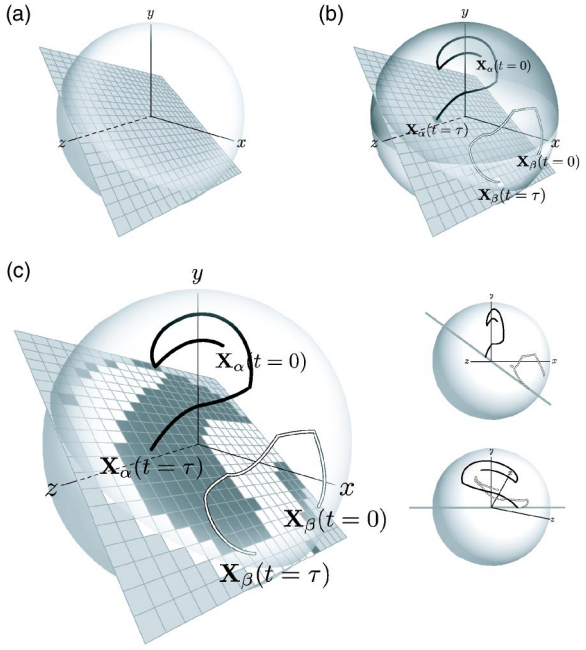

FIG. 5. A step-by-step illustration of the backtrace imaging procedure, which makes it possible to image any configuration of points in the droplet directly at an arbitrary time in the mixing process. Here we apply the technique to render a cross section within a droplet. (a) A uniform square grid of points is initialized at an arbitrary density in the desired spatial cross section. (b) Imagining that every fluid particle in the droplet is uniquely labeled, each grid point $\mathbf{x}$ corresponds to $\mathbf{X}_\alpha(t=\tau)$ for some particle α at time τ. We evolve each grid point $\mathbf{x}$ backwards in time through the sequence of mixing flows to find $\mathbf{X}_\alpha(t=0)$. For clarity, only two grid points are shown being traced backwards in time. The pair of spheres at the lower right of the figure show edge-on views of the grid to clarify the three-dimensional nature of the two trajectories shown. Using the initial condition that the droplet begins half black and half white, the color of particle α is defined by its location $\mathbf{X}_\alpha(t=0)$ in the initial distribution, and the two paths shown are colored accordingly. Since the grid point $\mathbf{x}$ corresponds to the particle α at a later time, it receives the color of particle α. (c) Applying this procedure to all grid points efficiently yields a uniformly colored cross section of arbitrary orientation and resolution through the droplet at time τ in the mixing process.

leaves gaps throughout the cross section, while the backtrace imaging technique colors the cross section uniformly to the resolution of the plotter.

Here we explain how the backtrace imaging procedure is used to render a cross section through the model droplet at an arbitrary elapsed time τ in the mixing cycle. As mentioned in Sec. II, we use the initial condition that one hemisphere of the droplet is filled with black fluid and the other hemisphere with white. The basic steps in the procedure are illustrated in Fig. 5. First, a uniform square grid is initialized in the desired spatial cross section with an arbitrary density of points. These grid points are considered to be Lagrangian fluid particles in the droplet at time τ, and the goal is to determine their colors as produced by a stirring process acting on the initial condition described above. The position of the particle labeled α at time t is denoted $\mathbf{X}_\alpha(t)$. We focus on a particular grid point $\mathbf{x}$, which corresponds to $\mathbf{X}_\alpha(t=\tau)$ for some particle α. The second step in the backtrace imaging procedure is to evolve the grid point $\mathbf{x}$ backwards in time through the sequence of mixing flows to find $\mathbf{X}_\alpha(t=0)$. Third, since the distribution of each color of fluid in the droplet at time $t=0$ is known, the color of particle α is assigned based on the location of $\mathbf{X}_\alpha(t=0)$ in the initial distribution. This also establishes the color of the corresponding grid point $\mathbf{x}$, which is just the particle α at a later time. Applying this procedure to all grid points efficiently yields a uniformly colored cross section of arbitrary resolution through the droplet at time τ in the mixing process. Furthermore, this procedure naturally generalizes to color any distribution of points in the droplet at any elapsed time; for example, we later use it to color a three-dimensional grid within the droplet. Thus, for a study of kinematical features, backtrace imaging is a general, efficient method for visualizing the time evolution of a three-dimensional mixing flow.

V. QUANTIFYING MIXING

It is not obvious how best to quantify the extent to which two fluids are mixed or stirred; for example, consider the cross section shown in Fig. 4. However, for purposes of comparison and, by extension, optimization, it is highly desirable to have a simple scalar measure of mixing. Many measures of mixing have been proposed in the past century, with early references dating back at least to the work by Gibbs. Krasnopolskaya *et al.* present an excellent historical discussion on the subject of quantifying mixing quality;[20] see also the work by Bigio and Stry.[21] A recent issue of *Philosophical Transactions of the Royal Society of London A* (Volume 362, 2004) is devoted to mixing, and the papers therein illustrate the variety of current approaches to the problem.

It should be noted that the challenges of quantifying mixing are somewhat different in experiments than in numerical studies of kinematical mixing. Images of mixing in

Downloaded 22 Jul 2005 to 128.103.60.225. Redistribution subject to AIP license or copyright, see http://pof.aip.org/pof/copyright.jsp

experimental systems often range continuously in intensity between two extremes, and techniques of quantifying mixing in experiments commonly rely on this continuous distribution of intensities. In our model system, however, the backtrace imaging process introduced in the preceding section produces grids of points that are labeled with one of two colors. To use quantification techniques akin to those from experiments, these grids have to be converted into intensity profiles, which can be accomplished by dividing the grid into small volumes and calculating the proportion of one color of fluid in each volume to produce an intensity value. Mixing can then be quantified, for example, by the intensity of segregation defined by Danckwerts,[22] which is discussed in detail in the context of kinematical mixing by Krasnopolskaya *et al.*[20] However, using the flows in Sec. III, our preliminary implementations of measures of this sort appeared to depend strongly on the size of the averaging volume chosen. For kinematical studies of the type reported here, we sought a quantitative scalar measure that did not require the specification of an averaging volume size and could be applied directly to two- or three-dimensional grids labeled with two different colors. In this section, we first illustrate the box-size dependence of the intensity of segregation measure as applied to the droplet system, and we then introduce a scalar measure that does not require the specification of an averaging volume size.

To test a widely used mixing measure in the context of the droplet system, we chose to implement the Danckwerts intensity of segregation measure[22] in the form presented by Krasnopolskaya *et al.*[20] We apply the intensity of segregation measure in two dimensions to the central cross section of the droplet. We begin with a uniform Cartesian grid of a fixed density colored by the backtrace imaging procedure, where the coloring corresponds to a particular set of model parameters and a given time τ. Using the notation of Krasnopolskaya *et al.*, we divide the central cross section S into N_δ nonoverlapping square boxes of a side length δ, giving each box an area $S_\delta = \delta^2$. The box size δ is specified as a percentage of the side length of the uniform backtrace grid. Wet let $S_b^{(n)}$ represent the area of black fluid inside box n, which we approximate by counting the number of black grid points in the box, and we compute the "density of distribution" $D_n = S_b^{(n)}/S_\delta$ for each box. Finally, we compute the intensity of segregation I, where averages are computed over all boxes:

$$I = \frac{\langle (D - \langle D \rangle)^2 \rangle}{\langle D \rangle (1 - \langle D \rangle)}. \tag{3}$$

Figure 6 displays the behavior of the intensity of segregation through time for a variety of different box sizes. The model parameters used in this computation were $\tau_s = 3$, $\tau_t = 3$, $\beta = 2/3$, and $\lambda = 1$, and the dimensionless time τ ranges from 0 to 80. The backtrace imaging grid contained 300×300 points, and the box sizes used were 1%, 2%, 4%, and 8% of 300. The intensity of segregation decreases in time, and the qualitative trend of the measure is the same for different box sizes, but the actual value of the intensity of segregation depends heavily on the box size chosen; these results are consistent with those reported by Krasnopolskaya *et al.*, e.g., Fig. 11b of Ref. 20. We desired a mixing measure that did not depend on the choice of an averaging volume size, and we will now present such a measure.

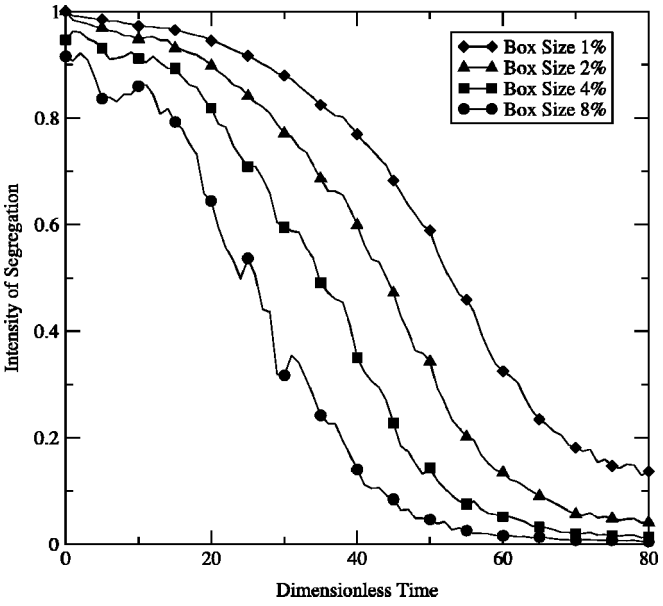

FIG. 6. The evolution of the Danckwerts intensity of segregation measure in time as applied in two dimensions to the central cross section of our model droplet. This measure requires the specification of an averaging volume size, or "box size," and we plot the intensity of segregation for several choices of box size. The model parameters used in this computation were $\tau_s = 3$, $\tau_t = 3$, $\beta = 2/3$, and $\lambda = 1$, and the dimensionless time τ ranges from 0 to 80. The visual time evolution of the central cross section for this set of parameters through $\tau = 40$ can be seen in Fig. 7 below. The backtrace imaging grid used here contained 300×300 points, and the box sizes used were 1%, 2%, 4%, and 8% of 300. Though the intensity of segregation follows the same qualitative trend for all box sizes tested, the quantitative variation of the measure over different box size choices is substantial.

The qualitative idea behind our mixing measure is to rank configurations of fluids in the droplet by how rapidly diffusion alone could homogenize them. To apply the measure, we begin either with a uniform two-dimensional Cartesian grid of points in a cross section of the droplet or with a uniform three-dimensional Cartesian grid of points that fills the entire droplet. Since the time it takes a particle to diffuse a distance δ is proportional to δ^2, we compute the minimum square Cartesian distance from each grid point to another of the *opposite* color and average this quantity over all grid points in the two- or three-dimensional region of interest to define a "mixing number." Though we do not implement diffusion in our simulations, diffusion is ultimately the primary mechanism of mixing on a molecular scale, which is why we choose this "δ^2" criterion to quantify mixing.

Here we define our mixing measure more formally. Consider a two-dimensional (2D) or three-dimensional (3D) uniform Cartesian grid colored by the backtrace imaging procedure defined above. Let the grid points $1 \ldots N$ be labeled x_i, and let $\mathrm{Opp}(x_i)$ denote the set of all grid points of color opposite to the color of point x_i. Also, let $d(x_i, x_j)$ denote the Cartesian distance from grid point x_i to grid point x_j (in 2D or 3D), and if S is a set of grid points, let $d(x_i, S) \equiv \min_j \{d(x_i, s_j)\}$, where $s_j \in S$ and $\min_j$ indicates a minimum taken over all s_j. We define the mixing measure $m(t)$

Downloaded 22 Jul 2005 to 128.103.60.225. Redistribution subject to AIP license or copyright, see http://pof.aip.org/pof/copyright.jsp

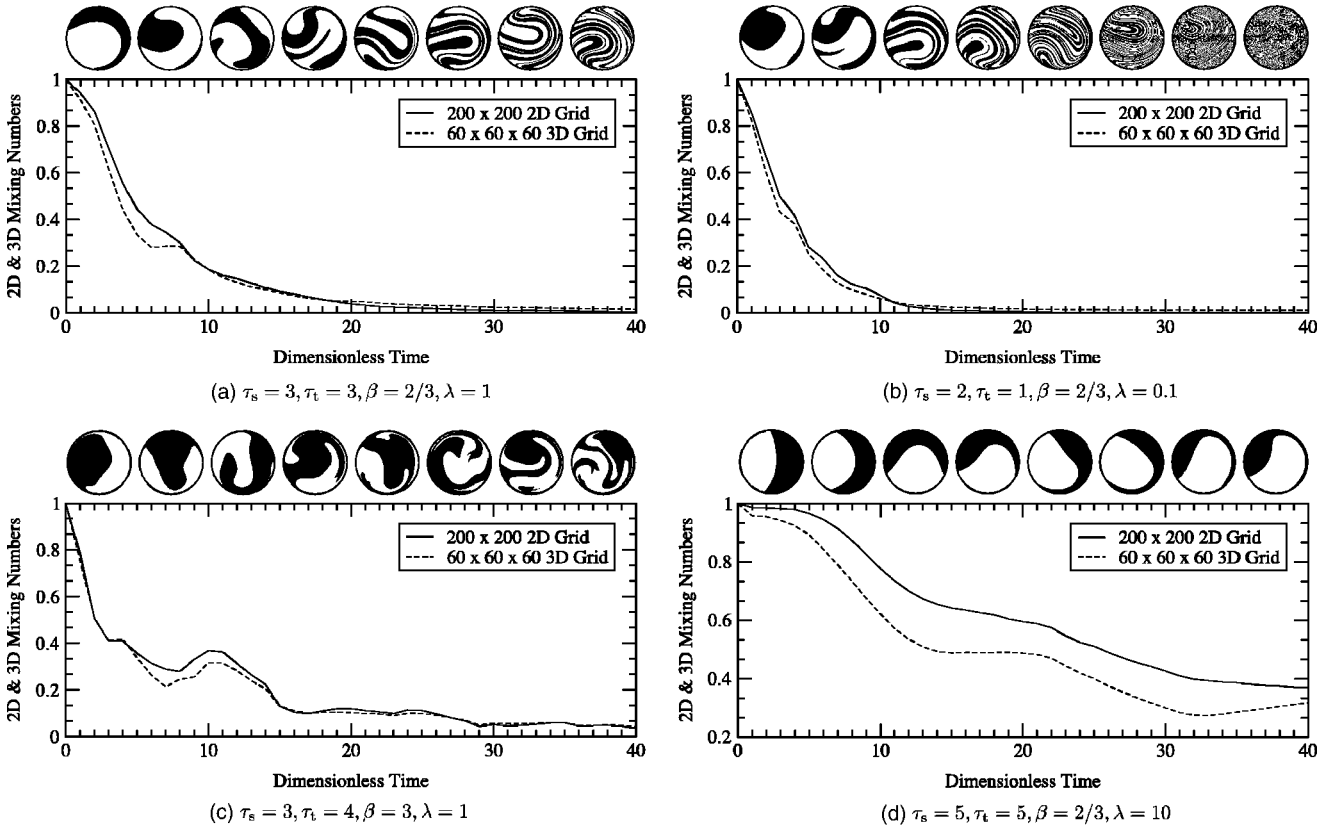

FIG. 7. The evolution in time of the central cross section and the normalized 2D and 3D mixing numbers, plotted with four sets of model parameters. In each sequence of cross sections, dimensionless time τ runs from 5 to 40 in increments of 5.

$$m(t) = \sum_{i=1}^{N} \frac{d^2(x_i, \mathrm{Opp}(x_i))}{N}. \tag{4}$$

If grids of finer and finer resolution are used to represent the same distribution, it is desired that m will converge to some value since it represents the degree of mixing in the droplet, and we illustrate this behavior in the following section. In each calculation, we first compute the mixing number for the initial ($t=0$) two- or three-dimensional droplet configuration and then normalize subsequent mixing numbers by that initial value.

To illustrate the two- and three-dimensional mixing measures defined by Eq. (4), we plot in Fig. 7 their evolution in time as our model droplet proceeds through mixing cycles representative of those described in Sec. III. We also present a sequence of images of the central cross section as it evolves in time to permit visual evaluation of the mixing.

The mixing number does depend on the grid spacing in the droplet, but in all of our simulations, we have found this dependence to be weak. Figure 8 plots the time evolution of the mixing number as calculated in the central cross section at four different grid resolutions using the parameters from Fig. 4. The mixing number appears to converge as the density of grid points in the droplet increases. We also plot the results as $\log(m)$ versus time to demonstrate that for this set of parameters, m decays approximately exponentially in time. Investigations are currently underway to determine whether the best-fit linear slope of $m(t)$ on a semilog plot can serve as a robust scalar quantifier of the *rate* of mixing.

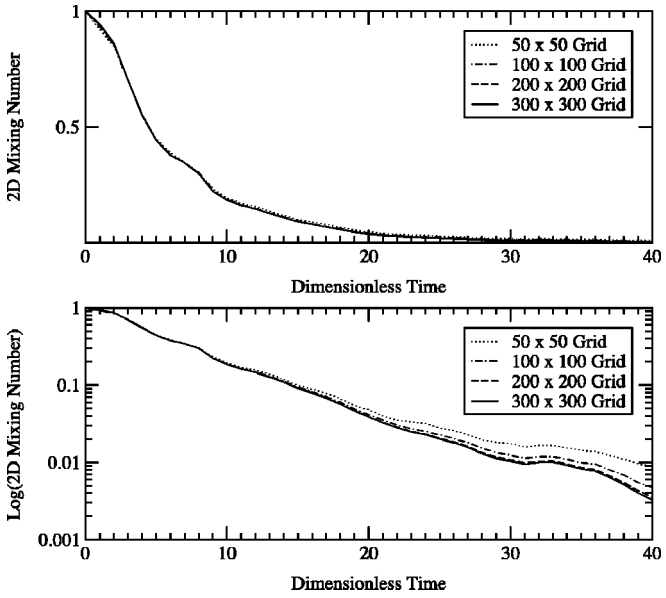

FIG. 8. The evolution of the normalized mixing number in time for four different grid resolutions: 50, 100, 200, and 300 grid points across the droplet. The value of the mixing number only weakly depends on the grid size, and its behavior in time is qualitatively the same at each resolution. The model parameters are $\tau_s=3$, $\tau_t=3$, $\beta=2/3$, and $\lambda=1$. The second plot, which is on a logarithmic scale, indicates that $\log(m) \sim -ct$ for this particular set of parameters.

Downloaded 22 Jul 2005 to 128.103.60.225. Redistribution subject to AIP license or copyright, see http://pof.aip.org/pof/copyright.jsp

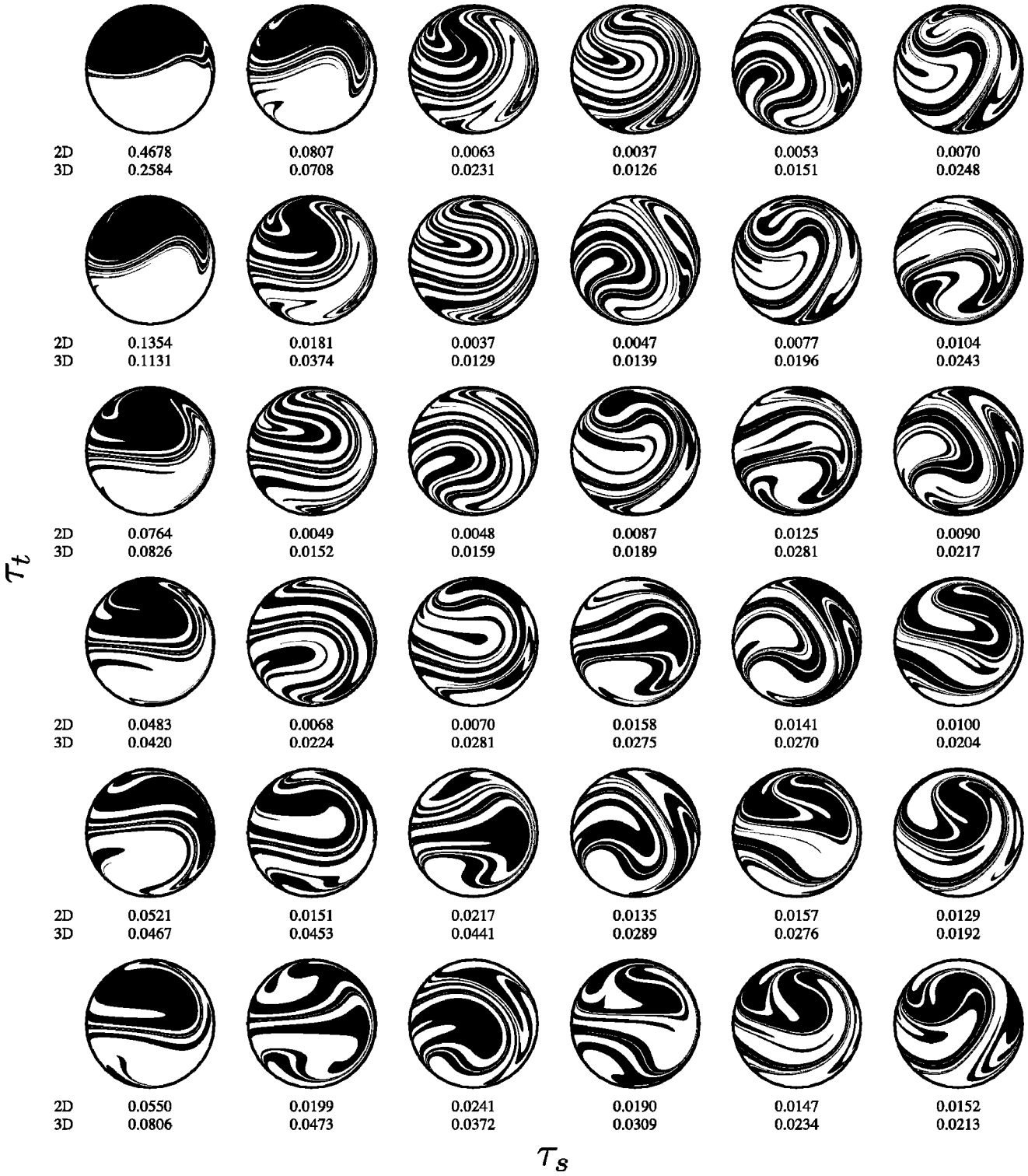

FIG. 9. The central cross section of the model droplet at $\tau=40$ for various pairs of τ_s and τ_t. The first line under each cross section is the 2D mixing number computed on a 100×100 grid, and the second line is the 3D mixing number computed on a $60\times60\times60$ grid. The parameter τ_s runs from 1 to 6 horizontally in the chart, and τ_t runs from 1 to 6 downwards. The other model parameters are fixed at $\beta=2/3$ and $\lambda=1$. The cross sections that appear well mixed visually also generally have the lowest mixing numbers.

VI. RESULTS AND DISCUSSION

It is generally important for mixing to proceed as rapidly as possible. To address the question of optimization in our model droplet mixer, we first fix some elapsed time τ in the mixing cycle at which to evaluate the extent of mixing. Next, we render charts of cross sections and their associated 2D and 3D mixing numbers at time τ for a range of model parameters. We do not attempt to find global optima since the full parameter space for our model is quite large; even in the case of a periodic mixing cycle, the parameters τ_s, τ_t, β, and

Downloaded 22 Jul 2005 to 128.103.60.225. Redistribution subject to AIP license or copyright, see http://pof.aip.org/pof/copyright.jsp

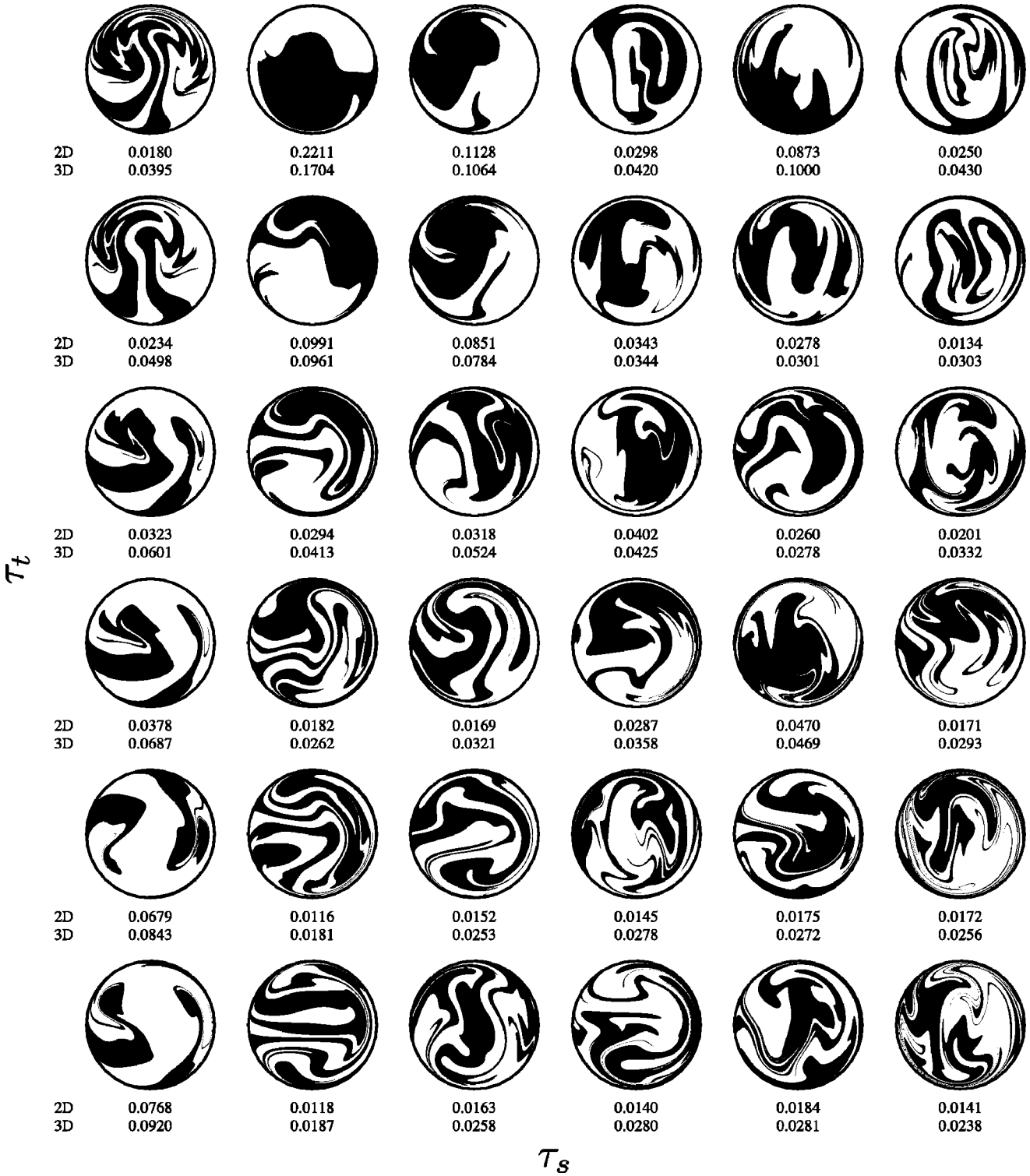

FIG. 10. Cross sections of the model droplet at $\tau=40$ for several pairs of τ_s and τ_t. The first line under each cross section is the 2D mixing number, and the second line is the 3D mixing number. The parameter τ_s runs from 1 to 6 horizontally in the chart, and τ_t runs from 1 to 6 downwards. The other model parameters are fixed at $\beta=5$ and $\lambda=1$.

λ can each be varied independently. If global optima were desired, it would be possible to use Newton's method or a similar algorithm to find minima of our mixing measure in the full four-dimensional parameter space. We choose to focus on approximate optimization of pairs of τ_s and τ_t for given values of β and λ.

In Fig. 9, we show the degree of mixing in the central ($x=0$) cross section of the droplet at $\tau=40$ as we systematically vary τ_s and τ_t between 1 and 6, fixing $\beta=2/3$ and $\lambda=1$. It is evident by visual inspection that the flows that mix best by $\tau=40$ are in a diagonal band that runs from $(\tau_s,\tau_t)=(4,1)$ to $(\tau_s,\tau_t)=(2,3)$, as those cross sections are filled

Downloaded 22 Jul 2005 to 128.103.60.225. Redistribution subject to AIP license or copyright, see http://pof.aip.org/pof/copyright.jsp

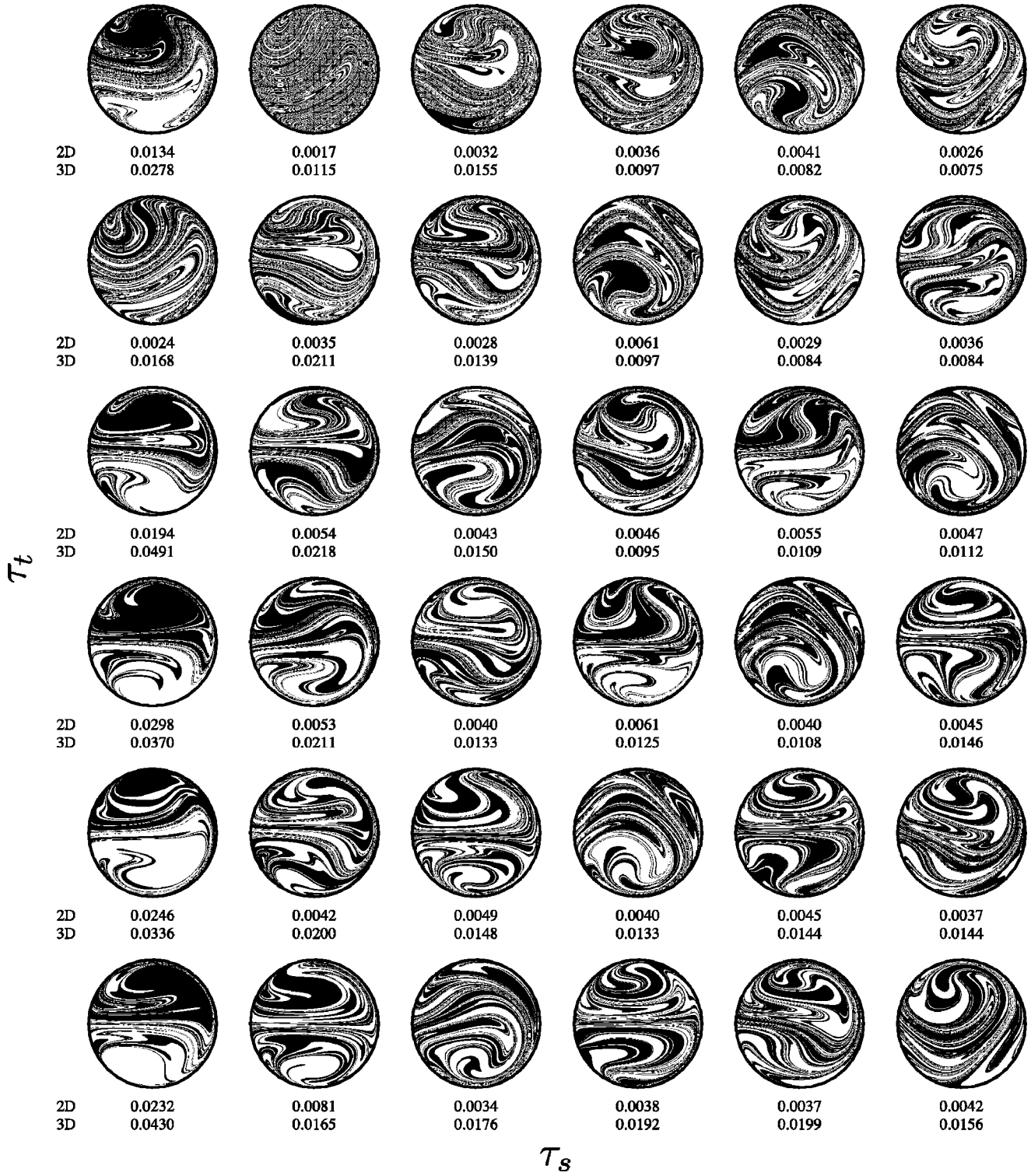

FIG. 11. Cross sections of the model droplet at $\tau=40$ for several pairs of τ_s and τ_t. The first line under each cross section is the 2D mixing number, and the second line is the 3D mixing number. The parameter τ_s runs from 1 to 6 horizontally in the chart, and τ_t runs from 1 to 6 downwards. The other model parameters are fixed at $\beta=2/3$ and $\lambda=0.1$.

with narrow striations of alternating color. The numbers under each image represent the degree of mixing, and they are calculated as described in Sec. V: the first value is the 2D mixing number evaluated directly on the cross section shown, and the second value is the 3D mixing number evaluated on a $60\times60\times60$ grid. Smaller values of m represent better mixing, and by inspection, both numerical measures of mixing are smallest in the band of cross sections that appear best-mixed visually.

The effect of increasing β (the dimensionless shear) to $\beta=5$ is illustrated in Fig. 10. All other parameters are the same as in Fig. 9. In this case, the values of m indicate that the best mixing occurs when $(\tau_s,\tau_t)=(2,5)$ and (2,6). A comparison of mixing numbers indicates that mixing is not as

Downloaded 22 Jul 2005 to 128.103.60.225. Redistribution subject to AIP license or copyright, see http://pof.aip.org/pof/copyright.jsp

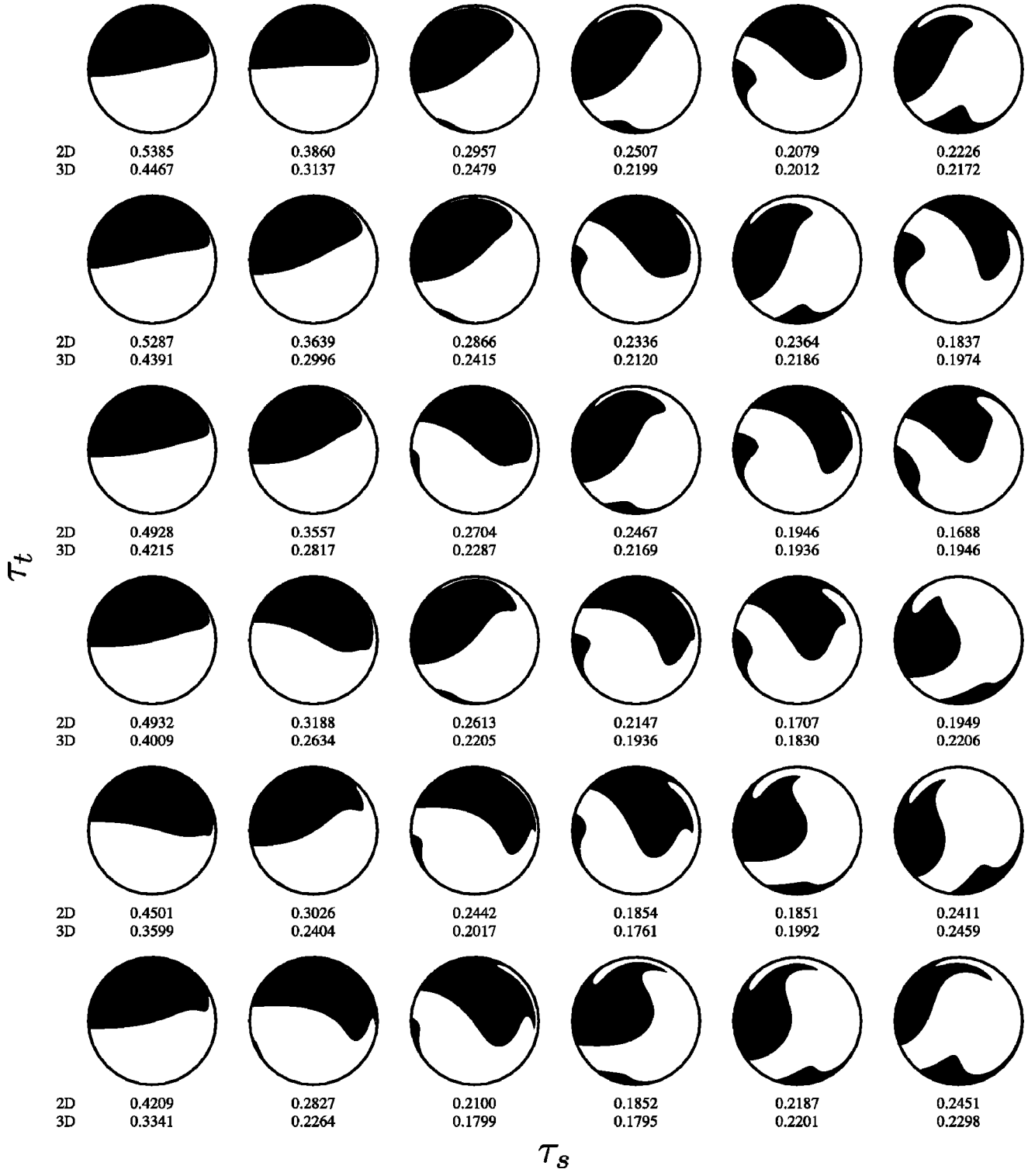

FIG. 12. Cross-sections of the model droplet at $\tau=40$ for several pairs of τ_s and τ_t. The first line under each cross section is the 2D mixing number, and the second line is the 3D mixing number. The parameter τ_s runs from 1 to 6 horizontally in the chart, and τ_t runs from 1 to 6 downwards. The other model parameters are fixed at $\beta=2/3$ and $\lambda=5$.

good as that in Fig. 9, which demonstrates that greater shear strength does not necessarily produce better mixing.

It is also of interest to study the effect of changing the viscosity ratio λ. In Fig. 11 we set $\lambda=0.1$, and in Fig. 12 we set $\lambda=5$. All other parameters retain their values from Fig. 9. Considering Figs. 9, 11, and 12 together, it appears that smaller values of λ, which correspond to smaller relative droplet viscosities, promote better mixing.

Finally, it is important to note that rankings of cross sections by the two-dimensional mixing number may not be identical to rankings by the three-dimensional mixing number. For example, the 3D mixing number of the (τ_s, τ_t)

Downloaded 22 Jul 2005 to 128.103.60.225. Redistribution subject to AIP license or copyright, see http://pof.aip.org/pof/copyright.jsp

$=(2,1)$ cross section in Fig. 11 is higher than the 3D mixing number of the $(\tau_s,\tau_t)=(4,2)$ cross section, even though the former cross section visually appears better mixed than the latter. We have examined representative examples of such cases more closely, and our findings indicate that the 3D mixing number accurately characterizes the full state of the droplet, which may be mixed better or worse overall than the central cross section suggests. Though the 2D and 3D mixing measures often display similar behavior, it can be misleading to quantify mixing solely by examining a single cross section.

VII. CONCLUSIONS AND FUTURE DIRECTIONS

We have presented a model droplet mixer that represents several flow features of the serpentine channel shown in Fig. 1. We described a backtrace imaging method that can render uniform cross sections of the droplet at arbitrary times in the mixing process, and we introduced a scalar measure of mixing that can be applied directly to a color-labeled two- or three-dimensional grid. The mixing measure qualitatively agreed with visual evaluation of mixing for all sets of parameters that we tested, and charts of cross sections and mixing numbers were used to compare mixing performance across large numbers of parameter sets. If desired, our mixing number could be used to search for global optima in the full parameter space of our model. In the parameter space that we explored, we found that the best mixing occurs when the viscosity ratio between the fluid inside the droplet and the surrounding fluid is small, which may have implications for the serpentine channel mixer.

This work could be extended in several ways. By computing the intensity of segregation and other mixing quantities alongside $m(t)$ for a variety of mixed droplets, it could be possible to identify the particular features of mixing that each scalar measure represents best. The near-exponential behavior of $m(t)$ in Fig. 8 is suggestive, and we intend to determine whether our measure behaves exponentially in time across a wide range of input parameters. If so, the slope of $m(t)$ on a semilog plot could serve as a scalar quantification of the rate of mixing, and we plan to determine whether it bears any relationship to the Lyapunov exponent. We also plan to test a variety of initial configurations of fluid in the droplet to determine the extent to which the behavior of $m(t)$ is independent of the initial fluid configuration.

We are in the process of studying a separate mixing measure based on the standard deviation of the d^2 values in Eq. (4), and we expect that measure will provide information about the sizes of unmixed regions of fluid in the droplet, much as Danckwerts's scale of segregation measure does.[22] It may also be interesting to generalize $m(t)$ to handle mixtures of three or more fluids, where coefficients could set the relative importance of proximity of any pair of fluid components.

ACKNOWLEDGMENTS

We thank R. Ismagilov and his colleagues at the University of Chicago for experimental data and helpful correspondence, and we are grateful to S. Wiggins for feedback on an early draft and extensive correspondence. We also thank D. Bigio, K. Jensen, T. Krasnopolskaya, I. Manas-Zloczower, V. Meleshko, I. Mezić, A. Stroock, T. Ward, and S. Lipoff for illuminating conversations. We acknowledge the Harvard MRSEC, the Harvard College Research Program, and the Harvard Physics Department for the support of this work.

[1] H. Aref, "Stirring by chaotic advection," J. Fluid Mech. **143**, 1 (1984).
[2] J. M. Ottino, *The Kinematics of Mixing: Stretching, Chaos, and Transport* (Cambridge University Press, New York, 1989).
[3] S. Wiggins and J. M. Ottino, "Foundations of chaotic mixing," Philos. Trans. R. Soc. London, Ser. A **362**, 937 (2004).
[4] A. D. Stroock, S. K. W. Dertinger, A. Ajdari, I. Mezic, H. A. Stone, and G. M. Whitsides, "Chaotic mixer for microchannels," Science **295**, 647 (2002).
[5] H. Song, J. D. Tice, and R. F. Ismagilov, "A microfluidic system for controlling reaction networks in time," Angew. Chem., Int. Ed. **42**, 767 (2003).
[6] K. Handique and M. A. Burns, "Mathematical modeling of drop mixing in a slit-type microchannel," J. Micromech. Microeng. **11**, 548 (2001).
[7] M. R. Bringer, C. J. Gerdts, H. Song, J. D. Tice, and R. F. Ismagilov, "Microfluidic systems for chemical kinetics that rely on chaotic mixing in droplets," Philos. Trans. R. Soc. London, Ser. A **362**, 1087 (2004).
[8] K. Bajer and H. K. Moffatt, "On a class of steady confined Stokes flows with chaotic streamlines," J. Fluid Mech. **212**, 337 (1990).
[9] H. A. Stone, A. Nadim, and S. H. Strogatz, "Chaotic streamlines inside drops immersed in steady Stokes flows," J. Fluid Mech. **232**, 629 (1991).
[10] D. Kroujiline and H. A. Stone, "Chaotic streamlines in steady bounded three-dimensional Stokes flows," Physica D **130**, 105 (1999).
[11] M. D. Bryden and H. Brenner, "Mass-transfer enhancement via chaotic laminar flow within a droplet," J. Fluid Mech. **379**, 319 (1999).
[12] T. Ward and G. M. Homsy, "Electrohydrodynamically driven chaotic mixing in a translating drop. II. Experiments," Phys. Fluids **15**, 2987 (2003).
[13] M. J. Martinez and K. S. Udell, "Axisymmetric creeping motion of drops through circular tubes," J. Fluid Mech. **210**, 565 (1990).
[14] M. Muradoglu and H. A. Stone, "Mixing in a drop moving through a serpentine channel: A computational study," Phys. Fluids (submitted).
[15] W. H. Press, B. P. Flannery, S. A. Teukolsky, and W. T. Vetterling, *Numerical Recipes in C: The Art of Scientific Computing* (Cambridge University Press, Cambridge UK, 1992).
[16] P. D. Swanson and J. M. Ottino, "A comparative computational and experimental study of chaotic mixing of viscous fluids," J. Fluid Mech. **213**, 227 (1990).
[17] A. J. S. Rodrigo, J. P. B. Mota, A. Lefèvre, and E. Saatdjian, "On the optimization of mixing protocol in a certain class of three-dimensional Stokes flows," Phys. Fluids **15**, 1505 (2003).
[18] A. D. Gilbert, "Magnetic field evolution in steady chaotic flows," Philos. Trans. R. Soc. London, Ser. A **339**, 627 (1992).
[19] W. Linxiang, F. Yurun, and C. Ying, "Animation of chaotic mixing by a backward Poincaré cell-map method," Int. J. Bifurcation and Chaos **11**, 1953 (2001).
[20] T. S. Krasnopolskaya, V. V. Meleshko, G. W. M. Peters, and H. E. H. Meijer, "Mixing in Stokes flow in an annular wedge cavity," Eur. J. Mech. B/Fluids **18**, 793 (1999).
[21] D. Bigio and W. Stry, "Measures of mixing in laminar flow," Polym. Eng. Sci. **30**, 153 (1990).
[22] P. V. Danckwerts, "The definition and measurement of some characteristics of mixtures," Appl. Sci. Res., Sect. A **3**, 279 (1952).

Downloaded 22 Jul 2005 to 128.103.60.225. Redistribution subject to AIP license or copyright, see http://pof.aip.org/pof/copyright.jsp